Editors' Suggestion | Featured in Physics

Multiple Galactic Sources with Emission Above 56 TeV Detected by HAWC

A. U. Abeysekara,[1] A. Albert,[2] R. Alfaro,[3] J. R. Angeles Camacho,[3] J. C. Arteaga-Velázquez,[4] K. P. Arunbabu,[5] D. Avila Rojas,[3] H. A. Ayala Solares,[6] V. Baghmanyan,[7] E. Belmont-Moreno,[3] S. Y. BenZvi,[8] C. Brisbois,[9] K. S. Caballero-Mora,[10] T. Capistrán,[11] A. Carramiñana,[11] S. Casanova,[7] U. Cotti,[4] J. Cotzomi,[12] S. Coutiño de León,[11] E. De la Fuente,[13,14] C. de León,[4] S. Dichiara,[15] B. L. Dingus,[2] M. A. DuVernois,[16] J. C. Díaz-Vélez,[13,14] R. W. Ellsworth,[9] K. Engel,[9] C. Espinoza,[3] H. Fleischhack,[17] N. Fraija,[15] A. Galván-Gámez,[15] D. Garcia,[3] J. A. García-González,[3] F. Garfias,[15] M. M. González,[15] J. A. Goodman,[9] J. P. Harding,[2] S. Hernandez,[3] J. Hinton,[18] B. Hona,[17] D. Huang,[17] F. Hueyotl-Zahuantitla,[10] P. Hüntemeyer,[17] A. Iriarte,[15] A. Jardin-Blicq,[18] V. Joshi,[19] S. Kaufmann,[20] D. Kieda,[1] A. Lara,[5] W. H. Lee,[15] H. León Vargas,[3] J. T. Linnemann,[21] A. L. Longinotti,[11] G. Luis-Raya,[20] J. Lundeen,[21] R. López-Coto,[22] K. Malone,[2,6,*] S. S. Marinelli,[21] O. Martinez,[12] I. Martinez-Castellanos,[9] J. Martínez-Castro,[23] H. Martínez-Huerta,[24] J. A. Matthews,[25] P. Miranda-Romagnoli,[26] J. A. Morales-Soto,[4] E. Moreno,[12] M. Mostafá,[6] A. Nayerhoda,[7] L. Nellen,[27] M. Newbold,[1] M. U. Nisa,[21] R. Noriega-Papaqui,[26] A. Peisker,[21] E. G. Pérez-Pérez,[20] J. Pretz,[6] Z. Ren,[25] C. D. Rho,[8] C. Rivière,[9] D. Rosa-González,[11] M. Rosenberg,[6] E. Ruiz-Velasco,[18] F. Salesa Greus,[7] A. Sandoval,[3] M. Schneider,[9] H. Schoorlemmer,[18] G. Sinnis,[2] A. J. Smith,[9] R. W. Springer,[1] P. Surajbali,[18] E. Tabachnick,[9] M. Tanner,[6] O. Tibolla,[20] K. Tollefson,[21] I. Torres,[11] R. Torres-Escobedo,[13,14] L. Villaseñor,[12] T. Weisgarber,[16] J. Wood,[28] T. Yapici,[8] H. Zhang,[29] and H. Zhou[2]

(HAWC Collaboration)

[1]*Department of Physics and Astronomy, University of Utah, Salt Lake City, Utah, USA*
[2]*Physics Division, Los Alamos National Laboratory, Los Alamos, New Mexico, USA*
[3]*Instituto de Física, Universidad Nacional Autónoma de México, Ciudad de Mexico, Mexico*
[4]*Universidad Michoacana de San Nicolás de Hidalgo, Morelia, Mexico*
[5]*Instituto de Geofísica, Universidad Nacional Autónoma de México, Ciudad de Mexico, Mexico*
[6]*Department of Physics, Pennsylvania State University, University Park, Pennsylvania, USA*
[7]*Institute of Nuclear Physics Polish Academy of Sciences, IFJ-PAN, Krakow, Poland*
[8]*Department of Physics & Astronomy, University of Rochester, Rochester, New York, USA*
[9]*Department of Physics, University of Maryland, College Park, Maryland, USA*
[10]*Universidad Autónoma de Chiapas, Tuxtla Gutiérrez, Chiapas, México*
[11]*Instituto Nacional de Astrofísica, Óptica y Electrónica, Puebla, Mexico*
[12]*Facultad de Ciencias Físico Matemáticas, Benemérita Universidad Autónoma de Puebla, Puebla, Mexico*
[13]*Departamento de Física, Centro Universitario de Ciencias Exactase Ingenierias, Universidad de Guadalajara, Guadalajara, Mexico*
[14]*Department of Physics and Astronomy, Texas Tech University, Lubbock, Texas, USA*
[15]*Instituto de Astronomía, Universidad Nacional Autónoma de México, Ciudad de Mexico, Mexico*
[16]*Department of Physics, University of Wisconsin-Madison, Madison, Wisconsin, USA*
[17]*Department of Physics, Michigan Technological University, Houghton, Michigan, USA*
[18]*Max-Planck Institute for Nuclear Physics, Heidelberg, Germany*
[19]*Erlangen Centre for Astroparticle Physics, Friedrich-Alexander-Universität Erlangen-Nürnberg, Erlangen, Germany*
[20]*Universidad Politecnica de Pachuca, Pachuca, Hgo, Mexico*
[21]*Department of Physics and Astronomy, Michigan State University, East Lansing, Michigan, USA*
[22]*INFN and Universita di Padova, via Marzolo 8, Padova, Italy*
[23]*Centro de Investigación en Computación, Instituto Politécnico Nacional, México City, México*
[24]*Instituto de Física de São Carlos, Universidade de São Paulo, São Carlos, São Paulo, Brasil*
[25]*Dept of Physics and Astronomy, University of New Mexico, Albuquerque, New Mexico, USA*
[26]*Universidad Autónoma del Estado de Hidalgo, Pachuca, Mexico*
[27]*Instituto de Ciencias Nucleares, Universidad Nacional Autónoma de Mexico, Ciudad de Mexico, Mexico*
[28]*NASA Marshall Space Flight Center, Hunstville, Alabama, USA*
[29]*Department of Physics and Astronomy, Purdue University, West Lafayette, Indiana, USA*

(Received 18 September 2019; revised manuscript received 21 November 2019; published 15 January 2020)

We present the first catalog of gamma-ray sources emitting above 56 and 100 TeV with data from the High Altitude Water Cherenkov Observatory, a wide field-of-view observatory capable of detecting gamma rays up to a few hundred TeV. Nine sources are observed above 56 TeV, all of which are likely galactic in

origin. Three sources continue emitting past 100 TeV, making this the highest-energy gamma-ray source catalog to date. We report the integral flux of each of these objects. We also report spectra for three highest-energy sources and discuss the possibility that they are PeVatrons.

DOI: 10.1103/PhysRevLett.124.021102

Introduction.—The all-particle cosmic-ray (CR) spectrum contains a break called the "knee" at ∼1 PeV [1]. CRs are expected to be galactic in origin up to at least this point. Identifying sources that accelerate particles to this energy ("PeVatrons") can help us understand this feature.

The question of which source classes can be PeVatrons is still open. Supernova remnants (SNRs) have traditionally been suggested as the most plausible candidates [2]. However, theories of CR acceleration in SNRs begin to encounter problems at a few hundred TeVs [3,4]. Alternative PeVatron candidates include young massive star clusters [5] and supermassive black holes [6]. The only previously reported PeVatron (the galactic center region, by the H.E.S.S. Collaboration [6]) has been hypothesized to be the latter. This source does not have a high enough current rate of particle acceleration to provide a sizable contribution to galactic CRs but could have been more active in the past.

Since CRs are charged, they bend in magnetic fields on their way to Earth and are difficult to trace back to their sources. Neutral gamma rays can instead be used to probe PeVatrons. When CRs interact with their environment (the interstellar medium, an ambient photon, or the gas/plasma of an SNR), the particles created include neutral pions. Each π^0 decays to two gamma rays. For a PeV CR, the gamma ray is approximately 1 order of magnitude less energetic [7]. A source with a hard gamma-ray spectrum (power-law index 2-2.4) extending to 100 TeV without an apparent spectral cutoff would be a clear signature of a PeVatron [2].

Charged pions, which are also created in these hadronic interactions, produce neutrinos. A subdominant ($< 14\%$) fraction of the IceCube astrophysical neutrinos [8,9] could be galactic in origin and also associated with PeVatrons [10]. Gamma-ray and neutrino measurements could be used together to probe PeVatrons.

Gamma rays are also produced via leptonic processes; at TeV energies, inverse Compton (IC) scattering is the dominant mechanism. Above a few tens of TeV, the leptonic component of gamma-ray emission becomes suppressed due to Klein-Nishina effects. This results in an energy-dependent spectral index [11]. Observations above 50 TeV are essential in identifying PeVatron candidates. If the spectrum of a source exhibits significant curvature, it is more likely to be dominated by leptonic emission.

Using data from the High Altitude Water Cherenkov (HAWC) Observatory [12,13], we present the highest-energy gamma-ray sky survey ever performed. HAWC is a wide field-of-view experiment that has unprecedented sensitivity at the highest photon energies [14] and excellent sensitivity to extended sources (the integral flux > 2 TeV is $\sim 10^{-13}$ cm^{-2} s^{-1} for a source extent of 0.5° [15]). These characteristics are crucial for detecting PeVatrons.

HAWC observations can also be used to look for signatures of Lorentz invariance violation (LIV). In some extensions of the Standard Model, the highest-energy photons decay quickly, with the decay probability near 100% over astrophysical distance scales [16,17]. Therefore, the existence of photons from astrophysical sources above 100 TeV constrains the linear effect of LIV to be $> 9.6 \times 10^{29}$ eV (78 times the Planck mass) [18]. This Letter focuses on the evidence of the sources detected by HAWC with $>$ 100 TeV photons. Further analysis of the highest-energy photons and their LIV implications will be discussed in a future publication.

Analysis method.—HAWC uses two recently developed energy estimation algorithms which have been used to identify > 56 TeV gamma rays from the Crab Nebula [19]. In this work, we use the "ground parameter" method. Throughout this Letter, $\hat{E}$ refers to estimated energy.

The analysis is performed in three steps: source identification, localization, and spectral fits. The data were collected between June 2015 and July 2018 (total live time: 1038.8 days). The background rejection, event binning, and likelihood framework [20] as described in [19] are used to create $\sqrt{\mathrm{TS}}$ [test statistic, defined as $-2\ln(\mathcal{L}_1/\mathcal{L}_0)$] (see the Supplemental Material [21]) maps of the high-energy sky above two $\hat{E}$ thresholds: 56 and 100 TeV. Sources in these maps are identified by applying the same technique used for the 2HWC catalog [22]. The declination range searched is −20°–60°. The maps are made assuming a power-law spectrum with an index of −2.0 and three different source morphology assumptions (point source as well as disks of radii 0.5° and 1.0°). The spectral index of −2.0 is chosen both because it is the standard index used in HAWC for studying extended sources [22] and because it is an expected index for PeVatrons.

A bright source may be found in the catalog search up to six times [22] (the three morphologies times two energy thresholds). To obtain one definitive source location and extension, the right ascension, declination, and extension are simultaneously fit for each source in the > 56 TeV map under the assumption of an $E^{-2.0}$ spectrum. These results are insensitive to the spectral index. A Gaussian spatial morphology is assumed. Because this is the first HAWC catalog constructed using maps with a high-energy threshold, we use the prefix "eHWC" (energy-HAWC) to identify the sources.

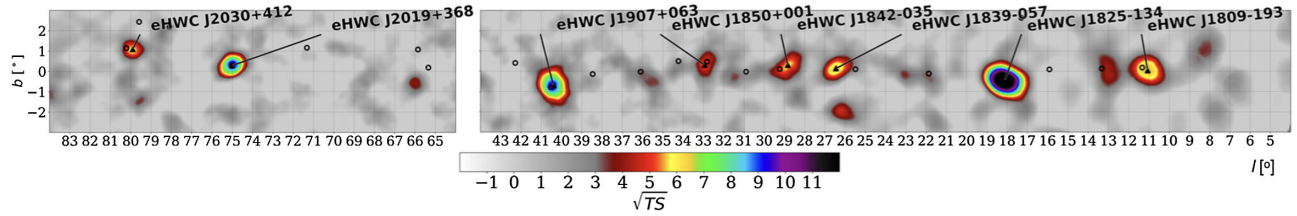

FIG. 1. $\sqrt{\mathrm{TS}}$ map of the galactic plane for $\hat{E} > 56$ TeV emission. A disk of radius 0.5° is assumed as the morphology. Black triangles denote the high-energy sources. For comparison, black open circles show sources from the 2HWC catalog.

The bins above 56 TeV are then fit to a power-law shape with the spectral index fixed to −2.7. The extent is fixed to the fitted high-energy extent. This index typically gives a higher TS value, possibly indicating a steepening of the spectra at the highest energies. The integral flux above 56 TeV is computed using the result of this fit. For sources that are significantly detected above an estimated energy of 100 TeV, spectral fits to the emission over the whole energy range accessible to HAWC are also performed using a binned-likelihood forward-folding technique that takes into account the angular response of the detector as well as the bias and energy resolution of the energy estimator.

When fitting the emission spectra of the sources, we do not consider multisource or multicomponent models; instead, we fit the spectrum in the region of interest (3° radius) while assuming Gaussian-shaped emission and allowing the value of the width to float. Contributions from diffuse emission and/or unresolved sources are not separated out. This introduces a systematic in the spectrum [22]. The integral flux values above 56 TeV are not expected to be affected since the diffuse emission falls rapidly with energy. In many cases, there are known to be two or more components to the emission, which may also affect the reported values of integral fluxes. For example, the eHWC J2030 + 412 region has contributions from both a pulsar wind nebula (PWN) and the possible TeV counterpart of the Fermi cocoon [23].

Results.—There are nine sources detected in the catalog search with significant ($\sqrt{\mathrm{TS}} > 5$) emission for $\hat{E} >$ 56 TeV (see Table S1 of the Supplemental Material [21] for the results of the search). Eight of these sources are within ∼1° of the galactic plane and are extended in apparent size (larger than HAWC's PSF) above this energy threshold. The only point source is the Crab Nebula (eHWC J0534 + 220), discussed in depth in [19]. Three of the sources show significant emission continuing above 100 TeV.

Figures 1 and 2 show $\sqrt{\mathrm{TS}}$ maps of the galactic plane for $\hat{E} > 56$ and > 100 TeV, respectively. For the Crab Nebula, see Fig. S1 in the Supplemental Material [21]. The sources are modeled as disks of radius 0.5°. Table I gives the integral flux for $\hat{E} > 56$ TeV for each source along with the fitted coordinates and Gaussian extension.

Most sources are within 0.5° of sources from the 2HWC catalog and, since they are extended, have overlapping emission. We previously estimated a false positive rate of 0.5 all-sky sources [22]. However, all of the sources discussed here are located close to the galactic plane and are consistent with previously known bright TeV sources, which makes them more likely to be the continuation of emission from lower energies than fluctuations.

Eight of the ten brightest sources from the 2HWC catalog are observed here. It is possible that ultrahigh-energy emission is a generic feature of astrophysical sources and more sources will be discovered as more data are collected and more sensitive experiments are built. This raises questions about emission mechanisms of astrophysical sources, especially if they are leptonic in origin (see Discussion).

Each source showing significant emission for $\hat{E} >$ 100 TeV is fit to three different spectral models: a power law, a power law with an exponential cutoff, and a log parabola. For eHWC J1825 − 134, the most-probable model (using the Bayesian information criterion [24]) is a power law with an exponential cutoff

$$\frac{dN}{dE} = \phi_0 \left(\frac{E}{10\ \mathrm{TeV}}\right)^{-\alpha} \exp(-E/E_{\mathrm{cut}}), \qquad (1)$$

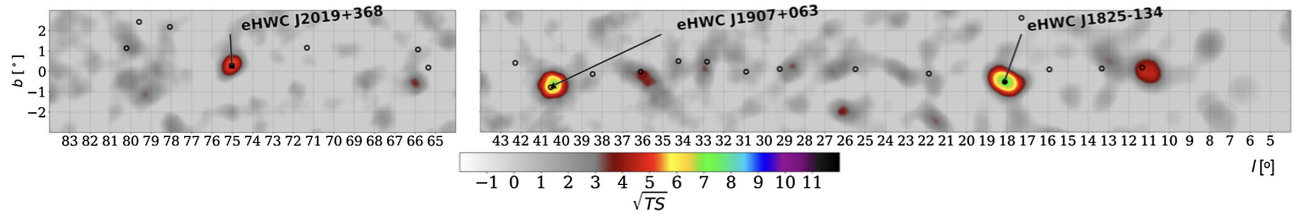

FIG. 2. The same as Fig. 1, but for $\hat{E} > 100$ TeV. The symbol convention is identical to Fig. 1.

TABLE I. Sources exhibiting $\hat{E} > 56$ TeV emission. A Gaussian morphology is assumed for a simultaneous fit to the source location and extension (68% Gaussian containment) for $\hat{E} > 56$ TeV. The integral flux F above 56 TeV is then fitted; $\sqrt{\mathrm{TS}}$ is the square root of the test statistic for the integral flux fit. The nearest source from the 2HWC catalog and the angular distance to it are also provided. In addition, the $\sqrt{\mathrm{TS}}$ of the same integral flux fit but above $\hat{E} > 100$ TeV is provided. All uncertainties are statistical only. The point spread function of HAWC for $\hat{E} > 56$ TeV is ~0.2° at the Crab declination [19], but is declination dependent and increases to 0.35° and 0.45° for eHWC J1825 − 134 and eHWC J1809 − 193, respectively. The overall pointing error is 0.1° [22].

Source name	RA (°)	Dec (°)	Extension > 56 TeV (°)	F (10^{-14} ph cm^{-2} s^{-1})	$\sqrt{\mathrm{TS}}$ > 56 TeV	Nearest 2HWC source	Distance to 2HWC source(°)	$\sqrt{\mathrm{TS}}$ > 100 TeV
eHWC J0534 + 220	83.61 ± 0.02	22.00 ± 0.03	PS	1.2 ± 0.2	12.0	J0534 + 220	0.02	4.44
eHWC J1809 − 193	272.46 ± 0.13	−19.34 ± 0.14	0.34 ± 0.13	$2.4^{+0.6}_{-0.5}$	6.97	J1809 − 190	0.30	4.82
eHWC J1825 − 134	276.40 ± 0.06	−13.37 ± 0.06	0.36 ± 0.05	4.6 ± 0.5	14.5	J1825 − 134	0.07	7.33
eHWC J1839 − 057	279.77 ± 0.12	−5.71 ± 0.10	0.34 ± 0.08	1.5 ± 0.3	7.03	J1837 − 065	0.96	3.06
eHWC J1842 − 035	280.72 ± 0.15	−3.51 ± 0.11	0.39 ± 0.09	1.5 ± 0.3	6.63	J1844 − 032	0.44	2.70
eHWC J1850 + 001	282.59 ± 0.21	0.14 ± 0.12	0.37 ± 0.16	$1.1^{+0.3}_{-0.2}$	5.31	J1849 + 001	0.20	3.04
eHWC J1907 + 063	286.91 ± 0.10	6.32 ± 0.09	0.52 ± 0.09	2.8 ± 0.4	10.4	J1908 + 063	0.16	7.30
eHWC J2019 + 368	304.95 ± 0.07	36.78 ± 0.04	0.20 ± 0.05	$1.6^{+0.3}_{-0.2}$	10.2	J2019 + 367	0.02	4.85
eHWC J2030 + 412	307.74 ± 0.09	41.23 ± 0.07	0.18 ± 0.06	0.9 ± 0.2	6.43	J2031 + 415	0.34	3.07

while eHWC J1907 + 063 and eHWC J2019 + 368 are better fit to log parabolas

$$\frac{dN}{dE} = \phi_0 \left(\frac{E}{10\ \mathrm{TeV}} \right)^{-\alpha - \beta \ln(E/10\ \mathrm{TeV})}. \quad (2)$$

All three sources are extended in apparent size over HAWC's entire energy range. Flux points are calculated for quarter-decade energy bins using the method described in [19]. When fitting the differential flux, it is assumed that the size of the source does not change with energy. Table II shows best-fit parameter values for these sources; Fig. 3 shows their spectra.

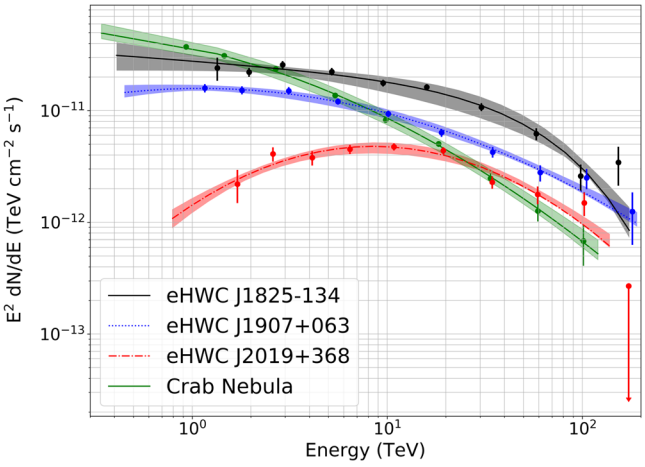

FIG. 3. The spectra of the three sources exhibiting significant $\hat{E} > 100$ TeV emission. For each source, the line is the overall forward-folded best fit. The error bars on the flux points are statistical uncertainties only. The shaded band around the overall best fit line shows the systematic uncertainties related to the HAWC detector model, as discussed in [19]. The Crab Nebula spectrum from [19] is shown for comparison.

We investigated whether the observed high-energy detections are compatible with being entirely due to misreconstructed events (see Tables S3 and S4 of the Supplemental Material [21]). For eHWC J1907 + 063, the strongest highest-energy detection, emission above a true energy of 56 TeV (100 TeV), is detected at the 7.6σ (4.6σ) level. Note that this is more conservative than the procedure followed in [25].

Each of the three > 100 TeV regions has also been observed by at least one of the imaging atmospheric Cherenkov telescopes (IACTs) (references: eHWC J1825 − 134 [26,27], eHWC J1907 + 063 [28,29], eHWC J2019 + 368 [30,31]). The HAWC measurements extend the energy range of these sources past 100 TeV for the first time. HAWC tends to measure higher fluxes (~2x difference) and larger source extents than the IACT measurements. These discrepancies cannot be explained by a misunderstanding of the HAWC detector response, as the HAWC spectrum of the Crab Nebula agrees with IACT measurements within uncertainties [19].

Both eHWC J2019 + 368 and eHWC J1825 − 134 have been separated into two or more sources by IACTs (see Table S8 of the Supplemental Material [21] for a list of TeVCat sources within 3° of each source), and the HAWC emission is the sum of these plus any additional unresolved sources. For example, eHWC J1825 − 134 overlaps with both HESS J1825 − 137 and HESS J1826 − 130. There are also differences in the computation of the background estimate [13,32], as well as the fact that contributions from diffuse emission are not considered here. This will be addressed in future Letters.

Discussion.—Although Klein-Nishina effects mean that any IC component of the emission becomes suppressed beginning around 10 TeV, merely detecting high-energy emission is not enough to claim a hadronic emission origin. The Crab Nebula is a firmly identified electron accelerator

TABLE II. Spectral fit values for the three sources that emit above 100 TeV. eHWC J1825 − 134 is fit to a power law with an exponential cutoff (Eq. (1); the other two sources are fit to a log parabola (Eq. (2). $\sqrt{\mathrm{TS}}$ is the square root of test statistic for the given likelihood spectral fit. Sources are modeled as a Gaussian; *extension* is the Gaussian width over the entire energy range. The uncertainties are statistical only. ϕ_0 is the flux normalization at the pivot energy (10 TeV). *PL diff* gives $\sqrt{\Delta\mathrm{TS}}$ between the given spectral model and a power law.

Source	$\sqrt{\mathrm{TS}}$	Extension (°)	ϕ_0 (10^{-13} TeV cm^2 s)$^{-1}$	α	E_{cut} (TeV)	PL diff
eHWC J1825 − 134	41.1	0.53 ± 0.02	2.12 ± 0.15	2.12 ± 0.06	61 ± 12	7.4
Source	$\sqrt{\mathrm{TS}}$	Extension (°)	ϕ_0 (10^{-13} TeV cm^2 s)$^{-1}$	α	β	PL diff
eHWC J1907 + 063	37.8	0.67 ± 0.03	0.95 ± 0.05	2.46 ± 0.03	0.11 ± 0.02	6.0
eHWC J2019 + 368	32.2	0.30 ± 0.02	0.45 ± 0.03	2.08 ± 0.06	0.26 ± 0.05	8.2

[33] that emits well past 100 TeV [19,25]. We consider both hadronic and leptonic emission mechanisms.

Leptonic emission mechanisms: All nine sources have at least one pulsar from the Australia Telsecope National Facility (ATNF) database [34] within 0.5° of the HAWC high-energy location (see Table III). Borrowing the terminology coined in [35,36], it has been suggested that these gamma-ray sources may be "TeV halos." The spatial extents of these objects are much larger than the x-ray PWN (∼25 pc) and the emission is leptonic in origin, stemming from electrons that have escaped the PWN radius [37]. For eight of these nine sources, at least one nearby pulsar has an extremely high spin-down power ($\dot{E} > 10^{36}$ erg/s). The distance between the center of the HAWC high-energy emission and the pulsar is generally less than the extent of the HAWC source.

There are only 26 high-$\dot{E}$ pulsars in the inner galactic plane ($|b| < 1°$ in galactic coordinates) and within HAWC's field of view (roughly $0° < l < 90°$). Depending on the spatial distribution of pulsars assumed, we expect only ∼1–2 pulsars to be within 0.5° of a HAWC high-energy source by chance. The Crab is not located in the inner galactic plane and is therefore excluded from this calculation, but is also associated with a high-$\dot{E}$ pulsar.

If these sources are all leptonic in nature, their extension raises interesting questions about particle diffusion as the highest-energy electrons are expected to cool very quickly, before traveling large distances.

The electrons that produce the gamma rays will also radiate synchrotron emission in x rays. To produce 100 TeV gamma rays on the cosmic microwave background requires electrons of ∼300 TeV, resulting in synchrotron emission peaking at 10 keV in a magnetic field of 3 microgauss [7]. Dedicated analyses including multiwavelength studies will be part of upcoming publications on individual objects.

TABLE III. Information on all pulsars with $\dot{E} > 10^{36}$ erg/s within 0.5° of each source. The only pulsar within 0.5° of eHWC J2030 + 412 has an $\dot{E}$ below this threshold; it is included here for completeness. All pulsar parameters come from the ATNF database, version 1.60 [34] unless specified. The distance between the pulsar and the HAWC source, as well as the HAWC high-energy source extent (from Table I), is given in parsecs here, assuming that the HAWC source is the same distance from the Earth as the pulsar.

HAWC source	PSR name	$\dot{E}$ (erg/s)	Age ($P/2\dot{P}$) (kyr)	Distance to Earth (kpc)	Distance between HAWC source and PSR [° (pc)]	HAWC source extent (pc)
eHWC J0534 + 220	J0534 + 2200	4.5×10^{38}	1.3	2.00	0.03 (1.05)	…
eHWC J1809 − 193	J1809 − 1917	1.8×10^{36}	51.3	3.27	0.05 (2.86)	19.4
…	J1811 − 1925	6.4×10^{36}	23.3	5.00	0.40 (34.9)	29.7
eHWC J1825 − 134	J1826 − 1334	2.8×10^{36}	21.4	3.61	0.26 (16.4)	22.1
…	J1826 − 1256	3.6×10^{36}	14.4	1.55	0.45 (12.2)	9.47
eHWC J1839 − 057	J1838 − 0537	6.0×10^{36}	4.89	2.0 [a]	0.10 (3.50)	11.9
eHWC J1842 − 035	J1844 − 0346	4.2×10^{36}	11.6	2.40 [b]	0.49 (20.5)	16.3
eHWC J1850 + 001	J1849 − 0001	9.8×10^{36}	42.9	7.00 [c]	0.37 (45.2)	45.2
eHWC J1907 + 063	J1907 + 0602	2.8×10^{36}	19.5	2.37	0.29 (12.0)	21.5
eHWC J2019 + 368	J2021 + 3651	3.4×10^{36}	17.2	1.80	0.27 (8.48)	6.28
eHWC J2030 + 412	J2032 + 4127	1.5×10^{35}	201	1.33	0.33 (7.66)	4.18

[a]Pseudodistance from [38].
[b]Pseudodistance from Eq. (3) of [39].
[c]Distance estimate from [40].

Hadronic emission mechanisms: Hadronic emission mechanisms could also contribute, even if the emission is dominantly leptonic. Assuming that these sources are connected to the pulsars, they are all fairly young, with the mean (median) characteristic age being 37 (20) kyr. This means that the observed TeV emission may include a contribution from a supernova remnant [35].

All three source spectra presented here either have a cutoff or curvature before 100 TeV, preventing their unambiguous identification as PeVatrons. However, this does not immediately disfavor the PeVatron hypothesis, since spectral curvature might already be present at tens of TeV [2] and additional steepening of the high-energy tails may be expected from pair production on the interstellar radiation field and the cosmic microwave background [41]. Additionally, the reported spectra here may include contributions from multiple sources, which makes it harder to interpret the cutoff as it relates to the nature of the gamma-ray emission.

If the emission is due to hadronic mechanisms, these gamma-ray sources may be potential neutrino sources [42]. Two sources are especially interesting which are as follows:

An IceCube search for pointlike sources in the astrophysical neutrino flux, the eHWC J1907 + 063 region had the second-best p value (although still consistent with a background-only hypothesis) in *a priori* defined source list motivated by gamma-ray observations [43]. The HAWC spectrum presented here, which has a relatively hard spectral index and less curvature than the other sources, provides hints of a hadronic component.

The eHWC J2030 + 412 region is coincident with the Cygnus OB2 complex, which is one of the young massive star clusters that has been previously suggested as a site of CR acceleration [5].

Conclusions.—We report HAWC observations of the highest-energy gamma-ray sources to date. There are nine sources with $\hat{E} > 56$ TeV emission; three also have significant $\hat{E} > 100$ TeV emission. Emission mechanisms are not yet clear, especially for eHWC J1825 − 134 and eHWC J1907 + 063. These are the two most significant sources above 100 TeV and both exhibit relatively hard spectra with extension at the highest energies, as expected for PeVatrons. Forthcoming HAWC observations of these sources [23,44,45] combined with multimessenger and multiwavelength studies will be important in disentangling emission mechanisms.

We acknowledge the support from the U.S. National Science Foundation; the U.S. Department of Energy Office of High-Energy Physics; the Laboratory Directed Research and Development program of Los Alamos National Laboratory; Consejo Nacional de Ciencia y Tecnología, México, Grants No. 271051, No. 232656, No. 260378, No. 179588, No. 254964, No. 258865, No. 243290, and No. 132197, A1-S-46288, cátedras 873, 1563, 341, 323, Red HAWC, México; DGAPA-UNAM Grants No. IG100317, No. IN111315, No. IN111716-3, No. IA102715, No. IN109916, No. IA102019, and No. IN112218; VIEP-BUAP; PIFI, PROFOCIE; the University of Wisconsin Alumni Research Foundation; the Institute of Geophysics, Planetary Physics, and Signatures at Los Alamos National Laboratory; Polish Science Centre, Grants No. DEC-2018/31/B/ST9/01069 and No. DEC-2017/27/B/ST9/02272; Coordinación de la Investigación Científica de la Universidad Michoacana; Royal Society—Newton Advanced Fellowship 180385. Thanks to Scott Delay, Luciano Díaz, and Eduardo Murrieta for technical support.

*kmalone@lanl.gov

[1] M. Tanabashi *et al.* (Particle Data Group), Phys. Rev. D **98**, 030001 (2018).
[2] F. A. Aharonian, Astropart. Phys. **43**, 71 (2013).
[3] S. Gabici, AIP Conf. Proc. **1792**, 020002 (2017).
[4] A. R. Bell, K. M. Schure, B. Reville, and G. Giacinti, Mon. Not. R. Astron. Soc. **431**, 415 (2013).
[5] F. Aharonian, R. Yang, and E. de Oña-Wilhelmi, Nat. Astron. **3**, 561 (2019).
[6] A. Abramowski, F. Aharonian, F. A. Benkhali, A. G. Akhperjanian, E. O. Anguner *et al.*, Nature (London) **531**, 476 (2016).
[7] J. Hinton and W. Hofmann, Annu. Rev. Astron. Astrophys. **47**, 523 (2009).
[8] M. G. Aartsen, R. Abbasi, Y. Abdou, M. Ackermann, J. Adams *et al.*, Science **342**, 1242856 (2013).
[9] M. G. Aartsen, M. Ackermann, J. Adams, J. A. Aguilar, M. Ahlers *et al.*, Phys. Rev. Lett. **113**, 101101 (2014).
[10] M. G. Aartsen, M. Ackermann, J. Adams, J. A. Aguilar, M. Ahlers, M. Ahrens *et al.*, Astrophys. J. **849**, 67 (2017).
[11] R. Moderski, M. Sikora, P. S. Coppi, and F. Aharonian, Mon. Not. R. Astron. Soc. **363**, 954 (2005).
[12] A. J. Smith, Proc. Sci., ICRC2015 (**2015**) 966.
[13] A. U. Abeysekara, R. Alfaro, C. Alvarez, J. D. Álvarez, R. Arceo *et al.*, Nucl. Instrum. Methods Phys. Res., Sect. A **888**, 138 (2018).
[14] A. U. Abeysekara, A. Albert, R. Alfaro, C. Alvarez, J. D. Álvarez *et al.*, Astrophys. J. **843**, 39 (2017).
[15] A. U. Abeysekara, R. Alfaro, C. Alvarez, J. D. Álvarez, R. Arceo *et al.*, Astropart. Phys. **50–52**, 26 (2013).
[16] H. Martínez-Huerta and A. Pérez-Lorenzana, Phys. Rev. D **95**, 063001 (2017).
[17] H. Martinez-Huerta, S. Marinelli, J. T. Linnemann, and J. Lundeen, Proc. Sci. ICRC2019 (**2019**) 738.
[18] H. Martínez-Huerta, Proc. Sci. ICRC2017 (**2017**) 868.
[19] A. U. Abeysekara, A. Albert, R. Alfaro, C. Alvarez, J. Alvarez *et al.*, Astrophys. J. **881**, 134 (2019).
[20] G. Vianello, R. J. Lauer, P. Younk, L. Tibaldo, J. M. Burgess, H. Ayala, P. Harding, M. Hui, N. Omodei, and H. Zhou, Proc. Sci. ICRC2015 (2015) 1042.
[21] See Supplemental Material at http://link.aps.org/supplemental/10.1103/PhysRevLett.124.021102 for information on the likelihood ratio test, full results of the catalog search, hard cutoff fits, and a list of known TeV sources close to each source.

[22] A. U. Abeysekara, A. Albert, R. Alfaro, C. Alvarez, J. D. Álvarez *et al.*, Astrophys. J. **843**, 40 (2017).
[23] B. Hona, H. Fleischhack, and P. Huentemeyer, Proc. Sci. ICRC2019 (**2019**) 699.
[24] G. Schwarz, Ann. Stat. **6**, 461 (1978).
[25] M. Amenomori, Y. W. Bao, X. J. Bi, D. Chen, T. L. Chen *et al.*, Phys. Rev. Lett. **123**, 051101 (2019).
[26] H. Abdalla, F. Aharonian, F. A. Benkhali, E. O. Angüner *et al.*, Astron. Astrophys. **621**, 18 (2019).
[27] E. O. Angüner, F. Aharonian, P. Bordas, S. Casanova, C. Hoischen, I. Oya, and A. Ziegler, AIP Conf. Proc. **1792**, 040024 (2017).
[28] E. Aliu, S. Archambault, T. Aune, B. Behera, M. Beilicke *et al.*, Astrophys. J. **787**, 166 (2014).
[29] F. Aharonian, A. Akhperjanian, G. Anton, U. De Barres Almeida, A. Bazer-Bachi *et al.*, Astron. Astrophys. **499**, 723 (2009).
[30] E. Aliu, T. Aune, B. Behera *et al.*, Astrophys. J. **788**, 78 (2014).
[31] A. U. Abeysekara, A. Archer, T. Aune, W. Benbow, R. Bird *et al.*, Astrophys. J. **861** (2018).
[32] A. Jardin-blicq, V. Marandon, and F. Brun, Proc. Sci. ICRC2019 (2019) 706.
[33] O. C. de Jager, A. K. Harding, P. F. Michelson, H. I. Nel, P. L. Nolan, P. Sreekumar, and D. J. Thompson, Astrophys. J. **457**, 253 (1996).
[34] R. N. Manchester, G. B. Hobbs, A. Teoh, and M. Hobbs, Astron. J. **129**, 1993 (2005).
[35] T. Linden, K. Auchettl, J. Bramante, I. Cholis, K. Fang, D. Hooper, T. Karwal, and S. W. Li, Phys. Rev. D **96**, 103016 (2017).
[36] T. Linden and B. J. Buckman, Phys. Rev. Lett. **120**, 121101 (2018).
[37] T. Sudoh, T. Linden, and J. F. Beacom, Phys. Rev. D **100**, 043016 (2019).
[38] H. J. Pletsch, L. Guillemot, B. Allen, M. Kramer, C. Aulbert *et al.*, Astrophys. J. Lett. **755**, L20 (2012).
[39] J. Wu, C. J. Clark, H. J. Pletsch, L. Guillemot, T. J. Johnson, P. Torne, D. J. Champion, and J. Deneva, Astrophys. J. **854**, 1 (2018).
[40] E. V. Gotthelf, J. P. Halpern, R. Terrier, and F. Mattana, Astrophys. J. Lett. **729**, L16 (2011).
[41] T. A. Porter, G. P. Rowell, G. Johannesson, and I. V. Moskalenko, Phys. Rev. D **98**, 041302(R) (2018).
[42] F. Halzen, A. Kheirandish, and V. Niro, Astropart. Phys. **86**, 46 (2017).
[43] M. G. Aartsen, M. Ackermann, J. Adams, J. A. Aguilar, M. Ahlers *et al.*, Eur. Phys. J. C **79**, 234 (2019).
[44] C. Brisbois and V. Joshi, Proc. Sci. ICRC2019 (**2019**) 639.
[45] F. Salesa Greus and S. Casanova, Proc. Sci. ICRC2019 (**2019**) 781.